Effects on Membrane Lateral Pressure Suggest Permeation Mechanisms for Bacterial Quorum Signaling Molecules

7 AUTHORS, INCLUDING:

Jacqueline Smith
Georgetown University
9 PUBLICATIONS **208** CITATIONS

SEE PROFILE

Jingxin Wang
Johns Hopkins University
24 PUBLICATIONS **498** CITATIONS

SEE PROFILE

Varnika Roy
University of Maryland, College Park
11 PUBLICATIONS **241** CITATIONS

SEE PROFILE

Herman O Sintim
University of Maryland, College Park
87 PUBLICATIONS **1,424** CITATIONS

SEE PROFILE

Effects on membrane lateral pressure suggest permeation mechanisms for bacterial quorum signaling molecules

Kishore Kamaraju[1], **Jacqueline Smith**[2], **Jingxin Wang**[2], **Varnika Roy**[3,4], **Herman O. Sintim**[2], **William E. Bentley**[3,4], and **Sergei Sukharev**[1,2,4]

Kishore Kamaraju: kamarajukishore@yahoo.com; Jacqueline Smith: jsmith48@umd.edu; Jingxin Wang: wjxin528@gmail.com; Varnika Roy: varnika.roy@gmail.com; Herman O. Sintim: hsintim@umd.edu; William E. Bentley: bentley@umd.edu; Sergei Sukharev: sukharev@umd.edu

[1]Department of Biology, University of Maryland, College Park, Maryland 20742

[2]Department of Chemistry and Biochemistry, University of Maryland, College Park, Maryland 20742

[3]Graduate Program in Molecular and Cell Biology, University of Maryland, College Park, Maryland 20742

[4]Fischell Department of Bioengineering, University of Maryland, College Park, Maryland 20742

Abstract

Quorum sensing is an intricate example of 'social' behavior in microbial communities mediated by small secreted molecules (autoinducers). The mechanisms of membrane permeation remain elusive for many of them. Here we present the assessment of membrane permeability for three natural autoinducers and five synthetic analogs based on their polarity, surface activity, affinity for lipid monolayers and ability to induce lateral pressure changes in the inner *E. coli* membrane sensed by the bacterial tension-activated channel MscS. AI-1 (N-(3-Oxodecanoyl)-L-homoserine lactone) is surface-active, it robustly inserts into lipid monolayers, indicating strong propensity toward membranes. When presented to membrane patches from the cytoplasmic side, AI-1 transiently shifts MscS's activation curve toward higher tensions due to intercalation into the cytoplasmic leaflet followed by redistribution to the opposite side. Indole showed no detectable surface activity at the air-water interface, but produced a moderate increase of lateral pressure in monolayers and was potent at shifting activation curves of MscS, demonstrating transients on sequential additions. AI-2 (4,5-dihydroxy-2,3-pentanedione, DPD) showed little activity at the interfaces, correspondingly with no effect on MscS activation. After chemical modification with isobutyl, hexyl or heptyl chains, AI-2 displayed strong surface activity. Hexyl and especially heptyl AI-2 induced robust transient shifts of MscS activation curves. The data strongly suggest that both AI-1 and indole are directly permeable through the membrane. AI-2, more hydrophilic, shows low affinity toward lipids and thus requires a transport system, whereas alkyl analogs of AI-2 should permeate the membrane directly.

Bacteria communicate with one another via the production, secretion and uptake of small signal molecules called autoinducers (AIs). This communication known as quorum sensing (QS) [1], synchronizes the activity of individual bacteria and coordinates multi-cellular level responses [2]. The intra and inter species communication networks are controlled by a diverse

set of interspecies and species-specific AIs. QS controls many bacterial phenotypes including motility, attachment, biofilm formation and secretion of virulence factors. There is increasing interest in developing QS inhibitors as next generation antimicrobials that can attenuate pathogenicity but are not bacteriostatic or bacteriocidal and thus, unlike the current antibiotic-based therapy, pose less evolutionary pressure to develop resistance [3]. Most of the anti-QS agents developed to date have been modeled on the natural AIs [4].

There is great diversity in the chemistry of AIs and in the modes by which these signals induce phenotypic changes. Some AIs bind to cognate receptor molecules on outer cell surfaces and initiate an information relay, others are actively or passively transported into the cytoplasm where they mediate transcriptional responses. To guide the effective design of next-generation anti-QS agents, it is imperative to identify not only pharmacophore units – the structures which antagonize QS signal reception and transduction, but also understand the transport mechanisms. In this study, we address the possibility of direct membrane permeation for three naturally occurring autoinducers: the *P. aeruginosa*-specific AI-1 [5], indole, an interspecies non-quorum signal [6,7], the universal auto-inducer AI-2 [8] and two alkylated synthetic analogs of AI-2.

The intra species signal AI-1 (acyl-homoserine lactone, AHL), consists of a set of alkyl chains of varying length, side-chain substitutions and backbone saturations, appended to the core lactone ring. The differences in the hydrophobic side chains provide intraspecies specificity to AI-1s [2]. In *Vibrio harveyi*, AHL-like signals are detected via two-component membrane bound histidine kinases [9,10]. In other species, AI-1 binds to LuxR-type cytosolic receptors, implying transport through the membrane [11,12]. To allow for direct permeation, the acyl groups should confer moderate affinity to the bilayer allowing traversing without strong accumulation in the lipid phase. AHL's with very long acyl chains may require active transport to cross the membrane, and multi-drug efflux pumps have been implicated in the export process [13]. Out of the many AHL signals known to date[14] we chose N-(3-Oxodecanoyl)-L-homoserine lactone that signals via the cytosolic LasIR circuit in the opportunistic human pathogen *Pseudomonas aeruginosa* [15,16].

AI-2 is a mixture of interconverting cyclic and linear isomers of 4,5-dihydroxy-2,3-pentanedione (DPD). AI-2 is produced in more than 70 species of bacteria [8] and plays a role in the virulence of many clinically relevant species [17–19], which makes it an important target for QS inhibition strategies. Generally polar, AI-2 is exported out of the cell through membrane-spanning transporters [20,21] and expected to be imported also through a facilitated mechanism. It has been shown that the *S. typhimurium* periplasmic protein LsrB binds to AI-2 and likely mediates its transport through an ABC-like transport system [22], while others have demonstrated that AI-2 still penetrates into LsrB mutant bacteria [23,24]. Ribose binding protein Rbs can also facilitate AI-2 uptake by bacteria [21]. Another possibility for AI-2 transport is direct membrane permeation. Thus the mechanism of AI-2 uptake is still a matter of debate. Membrane-permeable AI-2 analogs, which can freely diffuse into bacterial cells without the need for special transporters, have the potential to interrupt intracellular AI-2 mediated signaling.

Indole produced by many bacteria [6,7] is an interspecies signal which decreases biofilm formation in *E. coli* while *P. aeruginosa* increases biofilm formation in response to indole produced by *E. coli. acrEF* multidrug transporter efflux pumps have been implicated in indole export from the cell [25], but not much is known about the uptake mechanism. With the growing importance of indole as a phenotype regulator [26] it is timely to study its physical pathway into the bacterial cell.

Here we combine computational predictions, surface chemistry approaches and a new patch-clamp based technique utilizing the membrane-embedded mechanosensitive channel MscS as a lateral pressure sensor to determine whether AI-1, indole, AI-2 and its isobutyl, pentyl, hexyl and heptyl derivatives intercalate into the lipid bilayer, flip to the other side and thus enter the bacterial cell without any transport facilitator.

The oil/water or octanol/water partitioning coefficients (K_{OW}) have been common criteria for the assessment of membrane permeability [27]. In many cases K_{OW} can be accurately predicted just from the chemical structure [28,29]. Detailed studies of drug permeation, however, indicated that besides K_{OW} a simple surface activity (reduction of surface tension due to crowding at the air/water interface (Fig. 1A)) is a good corollary of permeability through the blood-brain barrier, the process that is also influenced by the cross-sectional area of the permeant molecule [30,31]. While silica-immobilized phospholipids[32] or liposomes[27] were used to quantify drug partitioning into lipids and lipid-impregnated filters were employed for direct permeability measurements [33], little information about drug partitioning into native membranes is currently available.

A highly useful measure of substance propensity toward lipids is the swelling of monomolecular lipid films (Langmuir monolayers) through intercalation of the amphipathic substance [34,35] measured as the increase of lateral pressure and/or molecular area (Fig. 1B). Mechanosensitive channels are also known to be sensitive to amphipathic substances [36–38]. Our previous study of several esters of parabenzoic acid has shown that the swelling of lipid monolayers directly correlates with the changes of lateral pressure in the inner *E. coli* membrane as indicated by shifts of activation curves of the mechanosensitive channel MscS on the tension scale [39]. The study demonstrated that MscS can be used as a sensor of lateral pressure in the bilayer since increased lateral pressure counteracts the membrane tension, the primary stimulus for channel activation (Fig. 1C). With its cytoplasmically positioned gate, the channel differentially senses changes of pressure in the inner and outer leaflets such that incorporation of an amphipath into the inner leaflet increases pressure on the gate causing right shift of the tension-activation curve, whereas periplasmic incorporation of the substance stretches the inner leaflet and shifts the curve towards lower tension [39,40]. Transient shifts of activation curves indicate initial asymmetry of incorporation and a time-dependent redistribution of the substance between the leaflets (Fig 1D), which typically returns the curve to its initial position. Persistent shifts of activation curves, on the other hand, may signify stable chemical gradients of intercalated species across the membrane [39]. This new technique provides a more direct information and complements the recently reported optical tracking of membrane insertion of several acyl-homoserine lactones using the dipole potential-sensitive dye di-8-ANEPPS [41].

MATERIALS AND METHODS

Chemical synthesis

DPD (AI-2) and hexyl AI-2 were prepared following a recently reported synthetic strategy [24,42]. Briefly, diazocarbonyls, readily generated from acetyl chloride or hexanoic acid chloride and diazomethane were reacted with a silyl-protected oxo-aldehyde under mild, catalytic DBU-conditions (DBU: 1,8-Diazabicyclo[5.4.0]undec-7-ene). The silyl protecting group on the products was then deprotected with TBAF (Tetrabutylammonium fluoride) and the diazodiols were oxidized with dimethyl dioxirane to afford DPD (acetyl chloride as starting material) or hexyl AI-2 (hexanoic acid chloride as starting material). Indole and AI-1 were purchased from Sigma-Aldrich (St Louis, MO). Since there were indications that AI-1 may convert into tetramic acid in bacteriological media and buffers [43], stock solutions were prepared in deionized water and mixed with recording buffers just prior to measurements. In a special experiment we determined that AI-1 is stable in pure water in

the course of several days, whereas in the phosphate buffer at pH 7.4 its half-life is 5.4 days (Fig. S1, supplement).

Computational analysis of structures

The chemical structures for the molecules were created using *WebLab ViewerPro* and *Chem3D*. The partial charges, dipole moments and electrostatic potential surfaces for the molecules were computed using *Gaussian 09* software on B3LYP/6-31G basis set. *WebLab ViewerPro* was used for calculating the cylindrical volumes of the molecules. *EPIWEB 4.0*, *ALOGPS 2.1* and *molinspiration* softwares were used to predict the octanol-water partion coefficient (K_{ow}), octanol-air partition coefficient (K_{oa}), solubility coefficient (S), volumes of the molecules and sum of surfaces of polar atoms [44,45].

Surface tension measurements and monolayer experiments

Surface tensions of sub-phase solutions containing different concentrations of indole, AI-1 or DPD were determined using the standard Wilhelmy method with a strip of filter paper (Whatman, No. 1, 10.5 mm wide and 0.25 mm thick) used as a plate. The subphase buffer consisted of 100 mM KCl, 5 mM KH_2PO_4 for experiments with indole while for others 5mM HEPES replaced the phosphate buffer and titrated with KOH to pH 7.4. The pressure sensor (model 601, NIMA, Coventry, UK) was pre-calibrated using a 100 mg weight, after which the surface tension of pure water was measured to be −72 mN/m. At this stage, the pressure sensor was set to zero and subsequent measurements of surface tension produced positive values of surface pressure. The surface activity data was fitted with the Gibbs isotherm to determine the molecular area, A_S, of the surface active substance at the air-water interface, $\frac{d\gamma}{d\ln C} = -RT\Gamma$, where $\Gamma = (N_A A_S)^{-1}$, where γ is the surface tension, C is the concentration of surface active substance in the aqueous phase, R is the gas constant, T – absolute temperature, Γ - surface excess and N_A - Avogadro constant. Extrapolating the fit to meet the horizontal line through the surface tension of solution devoid of the surface active substance (~ 72 mN/m) yields the apparent partition coefficient of the surface active molecule at air-water interface, K_{aw} [30]. Membrane partition coefficient, K_{memb}, is estimated with the values for A_S and K_{aw} [30,46].

A rectangular Teflon monolayer trough (total area ~550 cm^2) with a single movable barrier (NIMA) enclosed in an air-clean bench was used in all experiments with indole and AI-1 while those with DPD employed a smaller trough (total area ~20 cm^2). The surface pressures were measured with the same Wilhelmy method. *Escherichia coli* total polar lipid extract (TPE) in chloroform was purchased from Avanti Polar Lipids (Alabaster, AL). The procedure of lipid preparation included removal of chloroform under the stream of nitrogen in a pre-weighted glass vial followed by drying under vacuum for 1 hour. The vial was then carefully weighted and lipids were dissolved by vortexing in pure chloroform to a final concentration of 2 mM, (1.53 mg/ml for TPE). Spreading of lipids on the aqueous subphase was done using a gas-tight 50μl Hamilton syringe. The subphase buffer was the same as used for surface tension measurements (above). Due to limited solubility, indole was added into the pre-warmed (to about 60°C) subphase buffer to a desired concentration and thoroughly mixed on a stirring plate. Indole stably remained in solution after cooling to room temperature. AI-1 is insoluble in aqueous solution and a small amount of chloroform ~10 μl was used to dissolve AI-1 which was further mixed with aqueous solution to make 1.5 ml of stock solution of 10 mM. Even after the chloroform evaporated, AI-1 remained stable in the solution. DPD was readily soluble in aqueous solutions and the stock solution of 10 mM was stable over a few weeks. Pressure-area (π-A) isotherms were measured at room temperature (22° C) at a barrier speed of 20 cm^2/min on the larger (~550 cm^2) trough.

Electrophysiology

Giant *E. coli* spheroplasts were prepared by the standard technique [47] utilizing cephalexin as a cell septation blocker. The MJF 465 (*mscS⁻/mscK⁻/mscL⁻*) [48] strain was used to express WT MscS. Patch-clamp recordings of MscS were performed exactly as described by Akitake et al [49]. Electrodes were pulled from borosilicate capillaries to a bubble number of 4.5 (resistance 2.8 ± 0.2 MΩ, in a buffer of 39 mS/cm specific conductivity). Recordings were performed in symmetrical potassium (200mM KCl, 45mM $MgCl_2$, 5mM $CaCl_2$, 5mM HEPES titrated to pH 7.4 with KOH) buffers in the pipette and bath. The bath solution was same as the pipette solution with a 400mM sucrose supplement to osmotically stabilize spheroplasts. The signaling molecules were delivered into the bath through a laboratory-built perfusion system and the MscS activation midpoints were determined with 1 s ramp stimuli within 1 min of perfusion. Pressure ramps were applied using an HSPC-1 (ALA Scientific Instruments) high-speed pressure clamp apparatus [50] controlled via the analog output from the DigiData1320A. An ALA P-V unit upgraded with a stronger suction pump was used as the pressure and vacuum source. Vacuum and pressure were calibrated at both the pumps and the headstage using a PM015D pressure monitor (World Precision Instruments). Pressure traces were then recorded directly from the HSPC-1 head stage. Output commands to the HSPC-1 were controlled by Axon pClamp9 software (Axon Instruments) in episodic stimulation mode. The midpoint shifts of dose-response curves were analyzed using Clampfit (Axon Instruments).

RESULTS

The structures for AI-1, indole, AI-2 and its isobutyl and hexyl derivatives are presented in Fig. 2 along with the computed electrostatic maps, dipole moments and predicted octanol/ water partitioning coefficients. Chemical structures with computed partial charges for the three natural AIs are shown in supplemental Fig. S2, whereas structures for five alkylated derivatives of AI-2 in two inter-convertible (linear and lactol) forms are shown in Fig S3. The surface charge distribution of the molecule in aqueous environment shows that among the five molecules, AI-2 (DPD) is the most polar (49% of polar surface) with substantial partial charges distributed over most of the surface, and indole is most non-polar (11.5% of polar surface), but containing polarizable double bonds. AI-1 has an extended region of non-polar surface of the oxo-acyl chain separated from the polar hetero ring of the molecule. Segregation of polar and apolar areas in AI-1 suggests an amphipathic surfactant-like character orienting this molecule in the membrane with its own polar region adjacent to the phospholipid head groups and the hydrocarbon part aligning with those of the lipids. The dipole moment of the AI-1 headgroup (5.2 D) can potentially align against the dipole potential in the lipid layer [51] and the presence of NH group increases the hydrogen-bonding capacity additionally stabilizing its position. The alkylated derivatives of AI-2 also display amphipathic character, only with a smaller dipole. We ran the structures through three predicting programs to determine theoretical values for solubility and octanol-water partition coefficients for these molecules as a first step. The distribution of computed partial charges and predicted K_{ow} indicate that between indole and AI-1, AI-1 is the more hydrophobic while AI-2 is predicted to have preference for aqueous phase. AI-1 is predicted to be the most active at the air-water interface (Table 1). Indole with its polarizable double bonds may show a behavior intermediate between that of AI-2 and AI-1. The isobutyl, pentyl, hexyl and especially heptyl derivatives of AI-2 are predicted to be generally more oil-soluble.

Fig. 3 shows concentration-dependent changes of surface tension of aqueous buffer with the AIs and derivatives. Indole and AI-2 did not show any appreciable surface activity, while AI-1, isobutyl, hexyl and heptyl AI-2 decreased the surface tension of the solution by ~17 mN/m (at 1–5 mM). The positions of the curves indicate that AI-1 and the isobutyl AI-2 derivative are least hydrophobic while heptyl AI-2 is the most, with hexyl AI-2 having an

intermediate surface activity, consistent with the distributions of polar surfaces predicted from the structures (Table1). Notably, pentyl AI-2, in contrast to the isobutyl analog, did not show any measurable surface activity. The surface activity data were fitted in the linear region with the Gibbs isotherm to determine the surface excess (Γ), propensity toward air-water interface (K_{AW}), molecular area at the surface (A_S) and predict the membrane partitioning coefficient log K_{memb} [30,46], all presented in Table 1. The experimental logK_{aw} and calculated logK_{ow} show similar trends for isobutyl, hexyl and heptyl AI-2s. Change for logK_{ow} is 1.37 units for hexyl, and 1.84 for heptyl AI-2 relative to logK_{ow} of isobutyl AI-2. Experimental logK_{aw} increases by 0.63 units for hexyl, and 1.63 units for heptyl AI-2 relative to that of isobutyl AI-2. The calculated logK_{memb} similarly changes from 1.94 for AI-1 to 3.55 for heptyl AI-2, signifying increasing membrane propensity. The molecules occupy 49–57 Å^2 at the interface, the area comparable to that of condensed phospholipids in the bilayer.

To test whether the absence of surface activity of indole could be related to its low solubility in water, we pre-heated a 1 mM solution to 60–70°C to force complete dissolution. We then either diluted this solution 3, 10 or 30 fold into pure buffer at room temperature, or measured surface tension without dilution upon cooling. In neither case we observed a measurable decrease of surface tension.

Pressure-area (π-A) isotherms for lipid monolayers formed from *E. coli* total polar extract (TPE) with different concentrations of AI-1, indole and AI-2 in the subphase are shown in Fig. 4. At the far right end of abscissa (4A-C), the density of lipid molecules is low, resulting in no observable change in the surface pressure as seen for the control (0 mM) trace. With compression, lipids pack in an ordered two-dimensional film and a measurable change in the surface pressure occurs at around 140 Å^2/molecule. At the monolayer-bilayer equivalence pressure of 35 mN/m [52,53], the area per molecule for TPE is ~70 Å^2 [39], and the collapse is reproducibly observed at ~ 60 Å^2 when pressure exceeds 45 mN/m. No such variation in the surface pressure is observed in the absence of lipids for all concentrations of natural AIs in the buffer as the bulk-surface equilibrium for soluble surfactants is not affected by the position of the barrier. With indole or AI-2 present in the buffer, no changes in the surface pressure are observed at the extreme right, while AI-1 by itself brings about a concentration-dependent surface pressure increase as expected from the surface tension measurements at the air-water interface with no lipids. Between 70 and 150 Å^2/molecule, the isotherms experience both right- and up-shift relative to the control, with increasing concentration of the signaling molecule in the subphase. While no changes of surface tension at the air-water interface were observed for indole or AI-2, surface effects of these molecules were observed in the presence of lipids (Fig. 4B and C). At 35 mN/m, 1 mM AI-2 and indole bring about 2 and 5% increase in the lipid molecular area while AI-1 shows a greater and steeper increase (Fig. 4D). The bulk-surface equilibrium for indole and AI-2 clearly changes in the presence of lipid molecules. Near the collapse pressure of 45 mN/m, the traces for different concentrations of AIs essentially converge to the control trace implying that at these pressures AIs are reversibly 'squeezed-out' from the monolayer to the subphase. Divergence of traces at the monolayer-bilayer equivalence pressure for indole and especially AI-1 indicates that these species would be stably present among the lipids in the bilayer environment. The solubility of indole in the lipid matrix of the membrane was also shown by other techniques [13,54].

While the control π-A diagram in Fig.4A is smooth, the presence of AI-1 produces a shoulder (shown by an arrow) likely reflecting a transition associated with partitioning of AI-1 from the monolayer back to the subphase under increasing pressure. The onset of this transition near 100 Å^2 is almost independent of AI-1 concentration in the subphase, which suggests that in the expanded state of the film AI-1 can be associated with phospholipids at a

fixed stoichiometric ratio. Indeed, lipid area at collapse is about 60 $Å^2$ and the AI-1's estimated molecular area at the air-water interface is ~49 $Å^2$ (Table 1). From the molecular model, area of AI-1 can be as small as ~15 $Å^2$; but apparently the orientation of the molecule at the surface is larger or perhaps extra water is associated with AI-1. When a 60 $Å^2$ lipid molecule forms a 1:1 complex with AI-1, the resultant structure may compact to 100 $Å^2$ due to a steric fit or displacement of water [55]. When the monolayer is compressed below this area, AI-1 is gradually expelled to the bulk (Fig 4A). As dictated by the bulk-surface equilibrium, the expulsion takes more lateral pressure at higher concentrations of AI-1 in the subphase. The fact that the π-A diagrams converge with the control curve well above the monolayer-bilayer equivalence pressure indicates that substantial amount of AI-1 always remains in the monolayer and AI-1 should effectively intercalate into the lipid bilayer.

Previously, we have shown that MscS is sensitive to changes in the lateral pressure arising from partitioning of trifluoroethanol or parabens into the membranes [39,40]. In the following patch-clamp experiments we measured pressure midpoints ($p_{0.5}$) for MscS in native spheroplast patches in the presence of AIs. Fig. 5A shows the activation curves for a control patch and with 1 mM AI-1 presented from the cytoplasmic side. Soon after AI-1 addition to the bath (t=1 min), the activation curve shifts towards higher tension and then returns back to the control position over the course of ~15 min. Note the decrease in the maximum current recorded from the patch soon after the addition of AI-1, which is likely due to faster MscS inactivation under increased lateral pressure in the cytoplasmic leaflet acting on the gate (Fig. 1C). Inactivation was observed in every patch but varied between 10 and 60 % (n=11). Data from multiple patches provided the statistics for average shift of the activation midpoint in time for 1 mM AI-1 (Fig. 5B). Analogous behavior was previously observed with butyl paraben [39]. With time, not only the midpoint of activation curves returns to its initial position, but the full amplitude of response also recovers. This behavior can be interpreted as quick initial partitioning of AI-1 into the cytoplasmic leaflet that increases lateral pressure, shifting the activation curve to the right and simultaneously causing faster inactivation [39,40,56]. Within 10 min, AI-1 penetrates into the opposite side, equalizes pressures in both leaflets (Fig. 1D) returning system to the initial setpoint (Fig. 5B). The characteristic time of AI-1 redistribution within the bilayer is consistent with the previously reported rate of AI-1 permeation into intact bacteria [13]. Regarding the mechanism of MscS, the data confirms that the pressure asymmetry in the bilayer is the factor governing not only the tension sensitivity, but the rate of inactivation as well.

Indole (2.5 mM) presented to a naive patch from the cytoplasmic side also transiently shifts the activation curve by ~20% towards higher tension. In the course of 10–12 min, $p_{0.5}$ returns back and stabilizes at the level ~ 4% above the control (Fig. 5C). Fig. 5D shows data for the $p_{0.5}$ dynamics for four sequential additions of indole to the bath with 1 mM increments, separated by 12 min intervals. The right shift after each injection was followed by a return back to the control. The observed time course suggests that indole redistributes within the lipid bilayer with a characteristic time of 5–7 min.

No such effects were observed on the activation midpoint of MscS with AI-2 up to a concentration of 1 mM in the bath, indicating that either AI-2 does not partition into the membrane or the effects are within 5%, the normal control traces variation [49]. In order to confer stronger amphipathic character to the molecule we have modified the DPD backbone of AI-2 with isobutyl, n-pentyl, n-hexyl or n-heptyl chains in the 1-position (see Fig S2). Except for pentyl AI-2, all molecules showed a substantial propensity toward the air-water interface (Fig. 3) and 'swelling' of TPE monolayers. π-A isotherms (Fig. 6A) for isobutyl AI-2 converge earlier, near the monolayer-bilayer equivalence pressure (dashed line), whereas for the hexyl and heptyl forms the isotherms remain divergent above 35 mN/m. The

longer-chain form remains in the film more stably. The effect of pentyl AI-2 on surface pressure, however, was weaker than that of the isobutyl analog, and the isotherms (Fig. 6B) converged completely near 20 mN/m. Clearly it is not the number of carbons, but the shape of the hydrocarbon chain that matters more in this case. Increasing the number of carbons to six increases the effect on surface pressure (Fig 6C). Further extension of the alkyl chain to seven carbons qualitatively changes the behavior of amphiphilic AI-2 analogs at the air-water interface. While the surface pressure of hexyl AI-2 is independent of the position of the barrier, heptyl AI-2 by itself behaves more like an insoluble surfactant, showing a substantial increase of surface pressure with compression (Fig.6D, dotted line). Heptyl AI-2 has the strongest affinity to lipids and the π-A isotherm lies far above that of pure lipids, showing a ~26% increase of surface pressure at $68A^2$ per lipid molecule which corresponds to bilayer-like packing.

In patch-clamp experiments we did not see reproducible shifts of MscS's $p_{0.5}$ in the presence of 0.6–1 mM isobutyl or pentyl AI-2 (n=16, data not shown), but we observed substantial transient $p_{0.5}$ shifts with hexyl and heptyl AI-2s (Fig. 7), similar to those observed with AI-1. With hexyl AI-2, maximal transient shifts reached 20%, whereas heptyl AI-2 in ten times lower concentration produced up to 45% shifts in $p_{0.5}$, commensurate with its strongest effect on surface pressure (Fig. 6D).

DISCUSSION

The computed K_{ow} of the three natural bacterial signaling molecules AI-1, indole and AI-2, and the measured activities at the air-water interface initially suggested membrane partitioning for the most apolar/amphipathic AI-1, but gave no predictions regarding the other two as no changes of surface tension were detected. Monolayer experiments, however, revealed moderate swelling of lipid films in the presence of indole and even polar AI-2 indicating measurable affinity of both molecules toward phospholipids. The lipid environment is thus more attractive for indole and AI-2 than the bare air-water interface. Monolayers allow for probing substances for their propensities toward phospholipids at different packing densities. Increasing density/lateral pressure disfavors partitioning of the intercalating substance into the film [35], squeezing it back to the subphase (Figs. 4 and 6). The divergence of π-A isotherms at different concentrations of the tested substance reflects its affinity toward phospholipids, whereas the area differences at the bilayer-monolayer equivalence pressure may provide a measure of the equilibrium concentration of the substance in the membrane and the character of association with lipids [35,46].

Non-traditionally, we utilized the MscS channel as a sensor of lateral pressure in the membrane. MscS resides in the inner *E. coli* membrane, which is the main barrier for permeation. MscS perceives tension by its entire transmembrane domain, but since the gate is located more cytoplasmically [57,58], the channel is expected to be more sensitive to the pressure perturbations in the inner leaflet (Fig. 1), as was previously demonstrated for trifluoroethanol [40] and parabens [39]. Could the preferential sensitivity of MscS to tension in the cytoplasmic leaflet bear any physiological role? It is possible since new phospholipids are synthesized at the inner surface of the cytoplasmic membrane [59] and there must be a feedback regulating the rates of phospholipid insertion and peptidoglycan growth. MscS may potentially be a part of such mechanism.

The kinetics of MscS activation midpoint shifts upon unilateral addition of lipophilic AIs likely reflects two separate processes, the first is incorporation to the exposed cis-side of the membrane and the second is permeation to the trans-side. Because MscS detects the asymmetry between the leaflets, the rate of substance equilibration should not be too fast otherwise the transient shift may not be detected. The rates of both incorporation and

flipping to the other side may depend on the hydrophobicity of the substance and the nature of the polar group. AI-1 intercalates into the inner leaflet and shifts $p_{0.5}$ to the right by as much as 23% relative to untreated control (Fig. 5). This means that more tension is now needed to open the channel in order to overcome additional lateral pressure. Since the midpoint tension for MscS in native spheroplasts is 7.8 mN/m [56], a 23% shift (Fig. 5A) would correspond to about 1.8 mN/m which is of the same order of magnitude as the lateral pressure increase (~5 mN/m) observed in monolayers at the lipid area of 68–70 Å^2 corresponding to the packing density in the native membrane (Fig. 4A). Activation curves return back within 10–15 min of AI-1 addition providing the characteristic time of AI-1 redistribution into the outer leaflet which restores the symmetrical pressure profile. Permeation of AI-1 through cell membranes in this time frame was suggested by experiments on *Pseudomonas aerugenosa* [13]. The actual measurements of AI partitioning and redistribution presented here are done in *E. coli* spheroplasts which seem to serve as an adequate model of inner membranes of gram-negative bacteria. It has also been reported that *E. coli* responds to AI-1 released by *P. aeruginosa* [60], and the presented patch-clamp experiments exactly represent this real-life situation.

In contrast to AI-1, the propensity of AI-2 to monomolecular films was very subtle, and, correspondingly, we observed no detectable shifts of MscS' $p_{0.5}$ upon bath perfusion. This suggested that AI-2 should have limited permeability and must require a facilitated transport mechanism. Consistent with this notion, AI-2 was found to be a less efficient transcription activator in the *E. coli* strain (LW9) lacking the periplasmic LsrB component of the AI-2 transport system [24]. Derivatizing AI-2 with isobutyl, hexyl or heptyl chains conferred a pronounced surface activity (Fig. 3) which generally correlates with the ability to permeate membranes, but only the hexyl and heptyl forms caused substantial shifts of MscS $p_{0.5}$. The absence of transient $p_{0.5}$ shifts, however, does not mean that the isobutyl or pentyl forms are membrane-impermeable. Both forms crossed the membrane into bacterial cells devoid of the LsrB transporter and were effective inhibitors of LsrR-dependent transcription after phosphorylation [24]. Hexyl-DPD was independently shown to be a potent inhibitor of bioluminescence in *Vibrio harveyi* [61]. In fact, the less hydrophobic isobutyl form was more potent in *E. coli* [24]. Although the slightly higher efficacy of the isobutyl analog could be attributed to a variety of factors, such as tighter binding to LsrR, it is plausible that it also permeates faster as it is less effectively retained in the membrane and has smaller cross-sectional area. It is also possible that it quickly equilibrates between the leaflets producing a short-lived and hardly detectable change in $p_{0.5}$. Compared to the fluorescence-based technique of monitoring membrane partitioning of alkylated (C10-C14) AHL analogs [41], our method utilizing MscS as a lateral pressure sensor appears more direct as it is independent of the dipolar properties of the substance and readily detects relatively short-chain (C6 and C7) alkylated analogs in the membrane.

Based on previous studies [30,35,46,53] and the data presented above, it is safe to state that substances characterized with pronounced surface activity, affinity toward phospholipid monolayers and capable of transiently shifting MscS's $p_{0.5}$ are expected to permeate membranes well. With this regard, indole is an interesting example of substance with no surface activity, but apparently high membrane permeability. Indole favorably interacts with phospholipids not only due to hydrogen bonding through the nitrogen heteroatom [62], but also due to high overall polarizability of the molecule [54] and cation-π interactions [63]. Indole is the side chain of tryptophan, which in integral membrane proteins often faces the boundary between polar and apolar regions of the phospholipid bilayer [64]. NMR studies show indole's preferential distribution in the upper hydrocarbon-glycerol region of phospholipid bilayers [54]. Indole transiently shifts MscS $p_{0.5}$ and appears to cross the bilayer within 5–7 min. The headgroup layer was identified as the additional binding region due to cation-π interactions with the choline groups. In the case of *E. coli* phosphatidylcholine is

not the part of the system, but clearly is for *P. aerugenosa*[65]. It remains to be elucidated whether the headgroup of phosphatidyletholamine, the main *E. coli* phospholipid, can arrange for indole binding sites.

In conclusion, generation of new sets of molecules that can effectively antagonize QS systems must combine efforts to understand both the molecular bases for signal recognition and the transport mechanisms. We have characterized three naturally occurring autoinducers, AI-1, AI-2 and indole in terms of their ability to permeate membranes directly. Computations, surface activity measurements and monolayer experiments strongly suggested that *Pseudomonas*-specific AI-1 and indole are freely permeable, whereas the universal AI-2 should utilize a facilitated uptake mechanism possibly via a periplasmic receptor and membrane transporter [22]. The synthetic isobutyl, hexyl and heptyl analogs of AI-2 have properties similar to AI-1 and must be also membrane-permeable. Utilization of the mechanosensitive channel MscS as a sensor of lateral pressure asymmetry confirmed stable intercalation of AI-1, indole, hexyl and heptyl AI-2s into the inner bacterial membrane and estimated the characteristic time of traversing from one side to another. This new experimental approach detects the presence of the substance of interest in the native bacterial membrane and indicates the sidedness of initial intercalation and the direction of permeation. Our work thus suggests further strategies for targeted interventions into quorum sensing mechanisms that would free our efforts from searching for specific uptake systems for AI-1 or indole, but leave viable options of specifically targeting the systems responsible for the uptake of AI-2. On the other hand, our study fully justifies extensive searches for more hydrophobic analogs of AI-2 [24] that would freely permeate the cells and exert their effects on intracellular receptors or modifying enzymes.

Supplementary Material

Refer to Web version on PubMed Central for supplementary material.

Acknowledgments

Abbreviations

AI	autoinducer
AHL	acyl-homoserine lactone
DPD	4,5-dihydroxy-2,3-pentanedione,
MscS	mechanosensitive channel of small conductance
HSPC	high speed pressure clamp apparatus

Reference List

1. Fuqua WC, Winans SC, Greenberg EP. Quorum sensing in bacteria: the LuxR-LuxI family of cell density-responsive transcriptional regulators. J Bacteriol. 1994; 176(2):269–275. [PubMed: 8288518]

2. Waters CM, Bassler BL. Quorum sensing: cell-to-cell communication in bacteria. Annu Rev Cell Dev Biol. 2005; 21:319–346. [PubMed: 16212498]

3. Rasmussen TB, Givskov M. Quorum-sensing inhibitors as anti-pathogenic drugs. Int J Med Microbiol. 2006; 296(2–3):149–161. [PubMed: 16503194]

4. Sintim HO, Smith JA, Wang J, Nakayama S, Yan L. Paradigm shift in discovering next-generation anti-infective agents: targeting quorum sensing, c-di-GMP signaling and biofilm formation in bacteria with small molecules. Future Med Chem. 2010:1005–1035. [PubMed: 21426116]

5. De Kievit TR, Gillis R, Marx S, Brown C, Iglewski BH. Quorum-sensing genes in Pseudomonas aeruginosa biofilms: their role and expression patterns. Appl Environ Microbiol. 2001; 67(4):1865–1873. [PubMed: 11282644]

6. Wang D, Ding X, Rather PN. Indole can act as an extracellular signal in Escherichia coli. J Bacteriol. 2001; 183(14):4210–4216. [PubMed: 11418561]

7. Jayaraman A, Wood TK. Bacterial quorum sensing: signals, circuits, and implications for biofilms and disease. Annu Rev Biomed Eng. 2008; 10:145–167. [PubMed: 18647113]

8. Lowery CA, Dickerson TJ, Janda KD. Interspecies and interkingdom communication mediated by bacterial quorum sensing. Chem Soc Rev. 2008; 37(7):1337–1346. [PubMed: 18568160]

9. Novick RP, Projan SJ, Kornblum J, Ross HF, Ji G, Kreiswirth B, Vandenesch F, Moghazeh S. The agr P2 operon: an autocatalytic sensory transduction system in Staphylococcus aureus. Mol Gen Genet. 1995; 248(4):446–458. [PubMed: 7565609]

10. Henke JM, Bassler BL. Three parallel quorum-sensing systems regulate gene expression in Vibrio harveyi. J Bacteriol. 2004; 186(20):6902–6914. [PubMed: 15466044]

11. Fuqua C, Greenberg EP. Listening in on bacteria: acyl-homoserine lactone signalling. Nat Rev Mol Cell Biol. 2002; 3(9):685–695. [PubMed: 12209128]

12. Lowery CA, McKenzie KM, Qi L, Meijler MM, Janda KD. Quorum sensing in Vibrio harveyi: probing the specificity of the LuxP binding site. Bioorg Med Chem Lett. 2005; 15(9):2395–2398. [PubMed: 15837332]

13. Pearson JP, Van DC, Iglewski BH. Active efflux and diffusion are involved in transport of Pseudomonas aeruginosa cell-to-cell signals. J Bacteriol. 1999; 181(4):1203–1210. [PubMed: 9973347]

14. Charlton TS, de NR, Netting A, Kumar N, Hentzer M, Givskov M, Kjelleberg S. A novel and sensitive method for the quantification of N-3-oxoacyl homoserine lactones using gas chromatography-mass spectrometry: application to a model bacterial biofilm. Environ Microbiol. 2000; 2(5):530–541. [PubMed: 11233161]

15. Gambello MJ, Iglewski BH. Cloning and characterization of the Pseudomonas aeruginosa lasR gene, a transcriptional activator of elastase expression. J Bacteriol. 1991; 173(9):3000–3009. [PubMed: 1902216]

16. Passador L, Cook JM, Gambello MJ, Rust L, Iglewski BH. Expression of Pseudomonas aeruginosa virulence genes requires cell-to-cell communication. Science. 1993; 260(5111):1127–1130. [PubMed: 8493556]

17. Cloak OM, Solow BT, Briggs CE, Chen CY, Fratamico PM. Quorum sensing and production of autoinducer-2 in Campylobacter spp., Escherichia coli O157:H7, and Salmonella enterica serovar Typhimurium in foods. Appl Environ Microbiol. 2002; 68(9):4666–4671. [PubMed: 12200329]

18. Lee J, Bansal T, Jayaraman A, Bentley WE, Wood TK. Enterohemorrhagic Escherichia coli biofilms are inhibited by 7-hydroxyindole and stimulated by isatin. Appl Environ Microbiol. 2007; 73(13):4100–4109. [PubMed: 17483266]

19. Higgins DA, Pomianek ME, Kraml CM, Taylor RK, Semmelhack MF, Bassler BL. The major Vibrio cholerae autoinducer and its role in virulence factor production. Nature. 2007; 450(7171):883–886. [PubMed: 18004304]

20. Herzberg M, Kaye IK, Peti W, Wood TK. YdgG (TqsA) controls biofilm formation in Escherichia coli K-12 through autoinducer 2 transport. J Bacteriol. 2006; 188(2):587–598. [PubMed: 16385049]

21. James D, Shao H, Lamont RJ, Demuth DR. The Actinobacillus actinomycetemcomitans ribose binding protein RbsB interacts with cognate and heterologous autoinducer 2 signals. Infect Immun. 2006; 74(7):4021–4029. [PubMed: 16790775]

22. Miller ST, Xavier KB, Campagna SR, Taga ME, Semmelhack MF, Bassler BL, Hughson FM. Salmonella typhimurium recognizes a chemically distinct form of the bacterial quorum-sensing signal AI-2. Mol Cell. 2004; 15(5):677–687. [PubMed: 15350213]

23. Wang L, Li J, March JC, Valdes JJ, Bentley WE. luxS-dependent gene regulation in Escherichia coli K-12 revealed by genomic expression profiling. J Bacteriol. 2005; 187(24):8350–8360. [PubMed: 16321939]

24. Roy V, Smith JA, Wang J, Stewart JE, Bentley WE, Sintim HO. Synthetic analogs tailor native AI-2 signaling across bacterial species. J Am Chem Soc. 2010; 132(32):11141–11150. [PubMed: 20698680]

25. Kawamura-Sato K, Shibayama K, Horii T, Iimuma Y, Arakawa Y, Ohta M. Role of multiple efflux pumps in Escherichia coli in indole expulsion. FEMS Microbiol Lett. 1999; 179(2):345–352. [PubMed: 10518736]

26. Bansal T, Alaniz RC, Wood TK, Jayaraman A. The bacterial signal indole increases epithelial-cell tight-junction resistance and attenuates indicators of inflammation. Proc Natl Acad Sci U S A. 2010; 107(1):228–233. [PubMed: 19966295]

27. Ribeiro MM, Melo MN, Serrano ID, Santos NC, Castanho MA. Drug-lipid interaction evaluation: why a 19th century solution? Trends Pharmacol Sci. 2010

28. Livingstone DJ, Ford MG, Huuskonen JJ, Salt DW. Simultaneous prediction of aqueous solubility and octanol/water partition coefficient based on descriptors derived from molecular structure. J Comput Aided Mol Des. 2001; 15(8):741–752. [PubMed: 11718478]

29. Clark DE. In silico prediction of blood-brain barrier permeation. Drug Discov Today. 2003; 8(20): 927–933. [PubMed: 14554156]

30. Fischer H, Gottschlich R, Seelig A. Blood-brain barrier permeation: molecular parameters governing passive diffusion. J Membr Biol. 1998; 165(3):201–211. [PubMed: 9767674]

31. Seelig A, Gottschlich R, Devant RM. A method to determine the ability of drugs to diffuse through the blood-brain barrier. Proc Natl Acad Sci U S A. 1994; 91(1):68–72. [PubMed: 8278409]

32. Ong S, Liu H, Pidgeon C. Immobilized-artificial-membrane chromatography: measurements of membrane partition coefficient and predicting drug membrane permeability. J Chromatogr A. 1996; 728(1–2):113–128. [PubMed: 8673230]

33. Fischer H, Kansy M, Avdeef A, Senner F. Permeation of permanently positive charged molecules through artificial membranes--influence of physico-chemical properties. Eur J Pharm Sci. 2007; 31(1):32–42. [PubMed: 17416489]

34. Ibdah JA, Krebs KE, Phillips MC. The surface properties of apolipoproteins A-I and A-II at the lipid/water interface. Biochim Biophys Acta. 1989; 1004(3):300–308. [PubMed: 2503030]

35. Seelig A. The use of monolayers for simple and quantitative analysis of lipid-drug interactions exemplified with dibucaine and substance P. Cell Biol Int Rep. 1990; 14(4):369–380. [PubMed: 1693884]

36. Martinac B, Adler J, Kung C. Mechanosensitive ion channels of E. coli activated by amphipaths. Nature. 1990; 348(6298):261–263. [PubMed: 1700306]

37. Markin VS, Martinac B. Mechanosensitive ion channels as reporters of bilayer expansion. A theoretical model. Biophys J. 1991; 60(5):1120–1127. [PubMed: 1722115]

38. Perozo E, Kloda A, Cortes DM, Martinac B. Physical principles underlying the transduction of bilayer deformation forces during mechanosensitive channel gating. Nat Struct Biol. 2002; 9(9): 696–703. [PubMed: 12172537]

39. Kamaraju K, Sukharev S. The membrane lateral pressure-perturbing capacity of parabens and their effects on the mechanosensitive channel directly correlate with hydrophobicity. Biochemistry. 2008; 47(40):10540–10550. [PubMed: 18795793]

40. Akitake B, Spelbrink RE, Anishkin A, Killian JA, de KB, Sukharev S. 2,2,2-Trifluoroethanol changes the transition kinetics and subunit interactions in the small bacterial mechanosensitive channel MscS. Biophys J. 2007; 92(8):2771–2784. [PubMed: 17277184]

41. Davis BM, Jensen R, Williams P, O'Shea P. The interaction of N-acylhomoserine lactone quorum sensing signaling molecules with biological membranes: implications for inter-kingdom signaling. PLoS One. 2010; 5(10):e13522. [PubMed: 20975958]

42. Smith JA, Wang J, Nguyen-Mau SM, Lee V, Sintim HO. Biological screening of a diverse set of AI-2 analogues in Vibrio harveyi suggests that receptors which are involved in synergistic agonism of AI-2 and analogues are promiscuous. Chem Commun (Camb). 2009; (45):7033–7035. [PubMed: 19904385]

43. Kaufmann GF, Sartorio R, Lee SH, Rogers CJ, Meijler MM, Moss JA, Clapham B, Brogan AP, Dickerson TJ, Janda KD. Revisiting quorum sensing: Discovery of additional chemical and biological functions for 3-oxo-N-acylhomoserine lactones. Proc Natl Acad Sci U S A. 2005; 102(2):309–314. [PubMed: 15623555]

44. Ertl P, Rohde B, Selzer P. Fast calculation of molecular polar surface area as a sum of fragment-based contributions and its application to the prediction of drug transport properties. J Med Chem. 2000; 43(20):3714–3717. [PubMed: 11020286]

45. Tetko IV, Gasteiger J, Todeschini R, Mauri A, Livingstone D, Ertl P, Palyulin VA, Radchenko EV, Zefirov NS, Makarenko AS, Tanchuk VY, Prokopenko VV. Virtual computational chemistry laboratory--design and description. J Comput Aided Mol Des. 2005; 19(6):453–463. [PubMed: 16231203]

46. Suomalainen P, Johans C, Soderlund T, Kinnunen PK. Surface activity profiling of drugs applied to the prediction of blood-brain barrier permeability. J Med Chem. 2004; 47(7):1783–1788. [PubMed: 15027870]

47. Martinac B, Buechner M, Delcour AH, Adler J, Kung C. Pressure-sensitive ion channel in Escherichia coli. Proc Natl Acad Sci U S A. 1987; 84(8):2297–2301. [PubMed: 2436228]

48. Levina N, Totemeyer S, Stokes NR, Louis P, Jones MA, Booth IR. Protection of Escherichia coli cells against extreme turgor by activation of MscS and MscL mechanosensitive channels: identification of genes required for MscS activity. EMBO J. 1999; 18(7):1730–1737. [PubMed: 10202137]

49. Akitake B, Anishkin A, Sukharev S. The "dashpot" mechanism of stretch-dependent gating in MscS. J Gen Physiol. 2005; 125(2):143–154. [PubMed: 15657299]

50. Besch SR, Suchyna T, Sachs F. High-speed pressure clamp. Pflugers Arch. 2002; 445(1):161–166. [PubMed: 12397401]

51. Brockman H. Dipole Potential of Lipid-Membranes. Chemistry and Physics of Lipids. 1994; 73(1–2):57–79. [PubMed: 8001185]

52. Brockman H. Lipid monolayers: why use half a membrane to characterize protein-membrane interactions? Curr Opin Struct Biol. 1999; 9(4):438–443. [PubMed: 10449364]

53. Seelig A. Local anesthetics and pressure: a comparison of dibucaine binding to lipid monolayers and bilayers. Biochim Biophys Acta. 1987; 899(2):196–204. [PubMed: 3580365]

54. Gaede HC, Yau WM, Gawrisch K. Electrostatic contributions to indole-lipid interactions. J Phys Chem B. 2005; 109(26):13014–13023. [PubMed: 16852615]

55. Wolfe DH, Brockman HL. Regulation of the surface pressure of lipid monolayers and bilayers by the activity of water: derivation and application of an equation of state. Proc Natl Acad Sci U S A. 1988; 85(12):4285–4289. [PubMed: 3380792]

56. Belyy V, Kamaraju K, Akitake B, Anishkin A, Sukharev S. Adaptive behavior of bacterial mechanosensitive channels is coupled to membrane mechanics. J Gen Physiol. 2010; 135(6):641–652. [PubMed: 20513760]

57. Sotomayor M, Schulten K. Molecular dynamics study of gating in the mechanosensitive channel of small conductance MscS. Biophys J. 2004; 87(5):3050–3065. [PubMed: 15339798]

58. Anishkin A, Akitake B, Sukharev S. Characterization of the resting MscS: modeling and analysis of the closed bacterial mechanosensitive channel of small conductance. Biophys J. 2008; 94(4):1252–1266. [PubMed: 17981908]

59. Huijbregts RP, de Kroon AI, de KB. Topology and transport of membrane lipids in bacteria. Biochim Biophys Acta. 2000; 1469(1):43–61. [PubMed: 10692637]

60. Van HR, Aertsen A, Moons P, Vanoirbeek K, Michiels CW. N-acyl-L-homoserine lactone signal interception by Escherichia coli. FEMS Microbiol Lett. 2006; 256(1):83–89. [PubMed: 16487323]

61. Lowery CA, Abe T, Park J, Eubanks LM, Sawada D, Kaufmann GF, Janda KD. Revisiting AI-2 quorum sensing inhibitors: direct comparison of alkyl-DPD analogues and a natural product fimbrolide. J Am Chem Soc. 2009; 131(43):15584–15585. [PubMed: 19824634]

62. Babakhani A, Gorfe AA, Kim JE, McCammon JA. Thermodynamics of peptide insertion and aggregation in a lipid bilayer. J Phys Chem B. 2008; 112(34):10528–10534. [PubMed: 18681475]

63. Blaser G, Sanderson JM, Wilson MR. Free-energy relationships for the interactions of tryptophan with phosphocholines. Org Biomol Chem. 2009; 7(24):5119–5128. [PubMed: 20024107]

64. White SH, Wimley WC. Membrane protein folding and stability: physical principles. Annu Rev Biophys Biomol Struct. 1999; 28:319–365. [PubMed: 10410805]

65. Benamara H, Rihouey C, Jouenne T, Alexandre S. Impact of the biofilm mode of growth on the inner membrane phospholipid composition and lipid domains in Pseudomonas aeruginosa. Biochim Biophys Acta. 2011; 1808(1):98–105. [PubMed: 20849811]
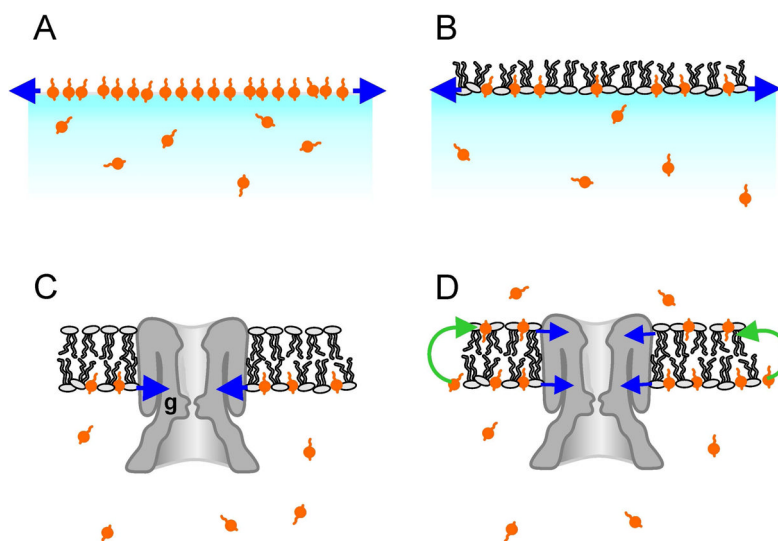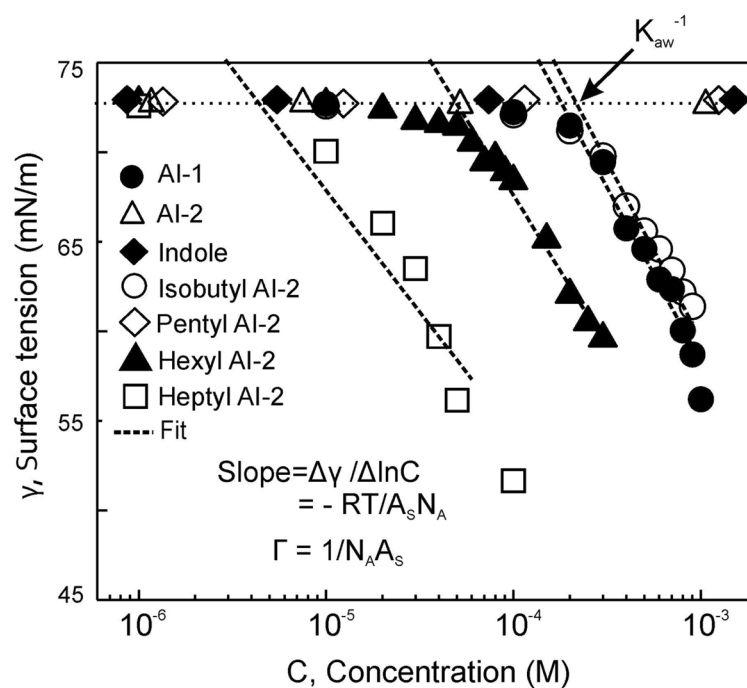
Figure 1.
Schematic representation of lateral pressures created by a surface-active substance at the air-water interface (A), upon intercalation into a lipid monolayer (B), in membrane patches under unilateral application and initial asymmetric distribution (C) and after re-distribution in the opposite monolayer (D). The gate of MscS channel (g) is located cytoplasmically near the boundary of the inner leaflet [58] and thus it experiences larger pressure with initial asymmetric distribution of the substance.
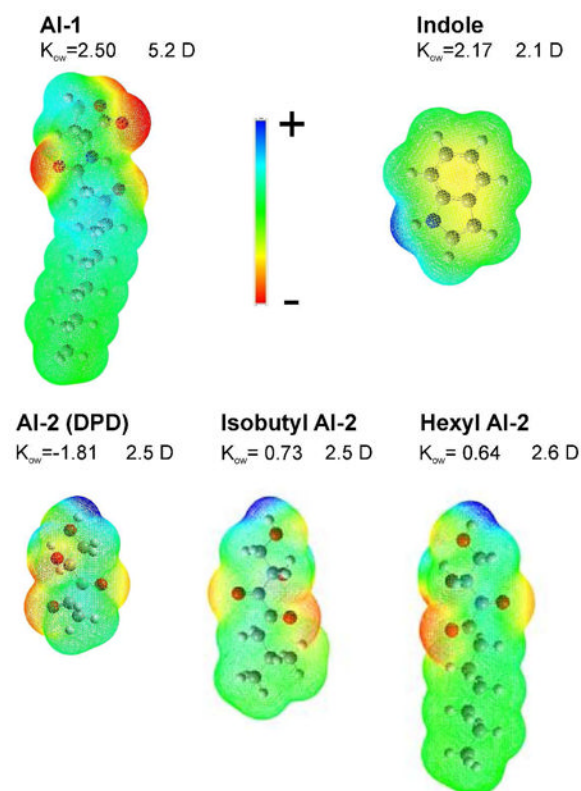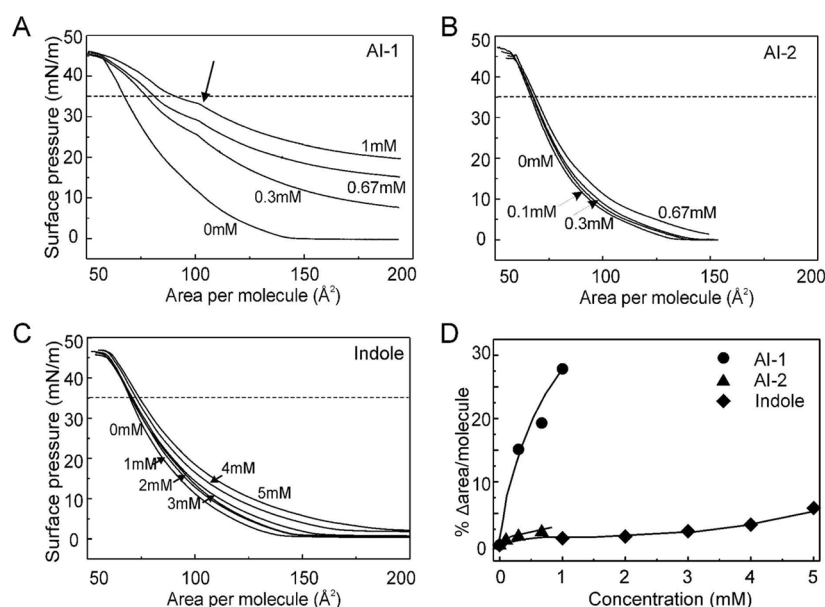
Figure 2.
Structures of AI-1, indole, AI-2 and isobutyl and hexyl derivatives of AI-2 (in the linear forms) with dipole moments and the electrostatic potential surfaces computed in *Gaussian*. The computed total surface and polar areas for these substances and two more alkylated analogs of AI-2 are presented in Table 1. Oil-water distribution coefficients K_{ow} are presented as averages of values from three prediction programs (see Methods). Chemical structures of these autoinducers including linear and cyclic (lactol) isomers of AI-2 and four alkylated analogs with computed partial charges are presented in the supplemental Figs. S1 and S2.
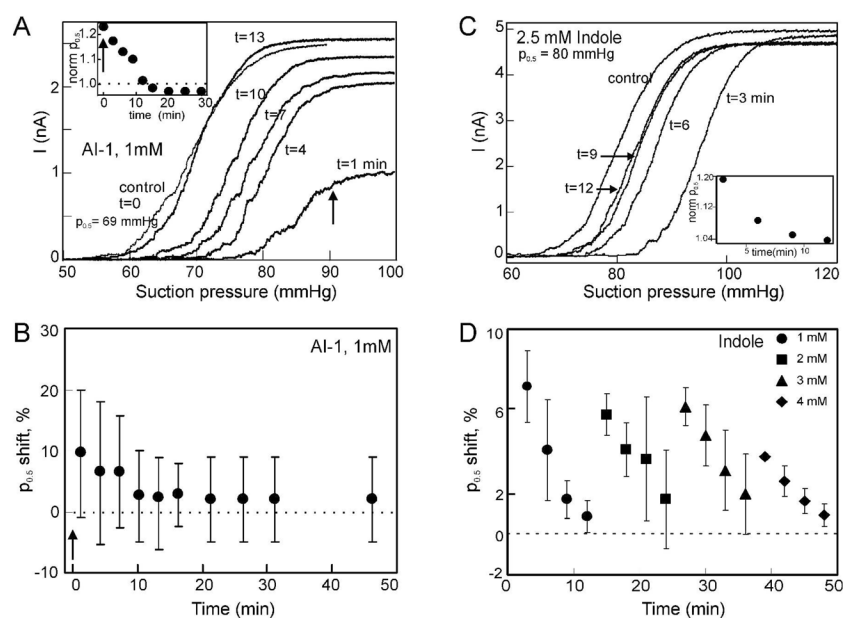
Figure 3.
Surface activity data for the three signaling molecules at the air-water interface. Straight lines show the fits of AI-1, isobutyl AI-2, pentyl, hexyl and heptyl AI-2 data using Gibbs isotherm. Pentyl AI-2 showed no measurable surface activity. Aqueous buffer solution: 100 mM KCl, 5 mM HEPES titrated with KOH to pH 7.4.

Figure 4.
Pressure-area isotherms from lipid monolayer experiments with natural autoinducers AI-1 (A), AI-2 (B) and indole (C) in the subphase. The dashed horizontal line designates the monolayer-bilayer equivalence pressure (35 mN/m). The arrow in (A) indicates the onset of a compacting transition reflecting pressure-driven expulsion of AI-1 from the film. Films were formed from the total polar *E. coli* extract (TPE) mimicking the composition of the inner membrane. Increase in lipid molecular area as a function of concentration of the signaling molecule at 35 mN/m (D).

Figure 5.
Transient shifts of MscS activation curves in response to AI-1 or Indole presented from the cytoplasmic side. (A) Effect of 1 mM AI-1. Activation midpoints ($p_{0.5}$) normalized to the control measured prior to AI-1 addition are shown as inset. (B) Averaged shifts of normalized $p_{0.5}$ as a function of time from multiple patches (n=11). (C) Effects of 2.5mM Indole with normalized p0.5 activation midpoints shown in inset. (D) Normalized averaged shifts of $p_{0.5}$ for sequential increase in concentration of indole as a function of time from multiple patches (n=6). All recordings were done in excised inside-out patches.
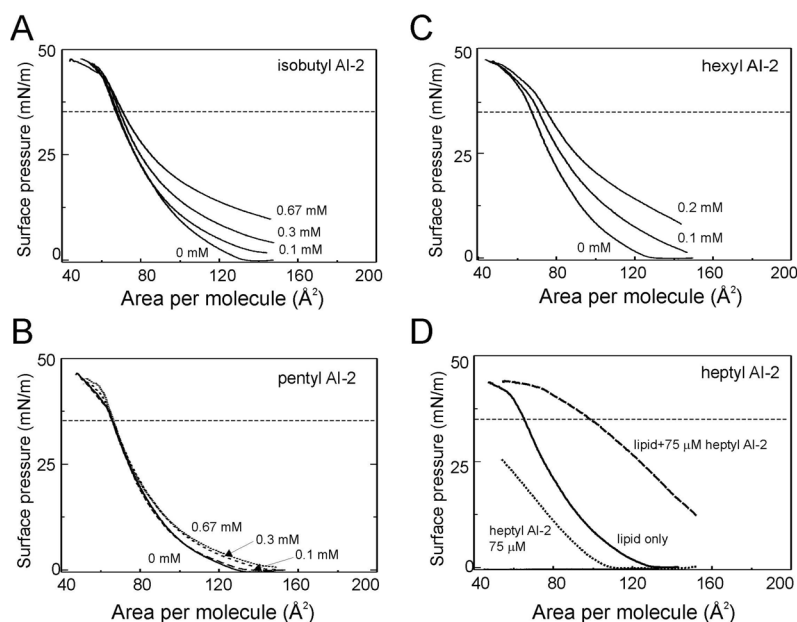
Fig. 6.
Monolayer data for four alkylated AI-2 derivatives. The measurements are taken in different ranges of concentrations, commensurate with the solubilities and magnitudes of effects. Isobutyl AI-2 exrets stronger effect on surface pressure that pentyl AI-2 (B) suggesting that branching matters more than the number of carbons in the alkyl chain. Increase of the number of carbons from six to seven qualitatively changes the behavior of the amphiphile at the air-water interface. Hexyl AI-2 (C) shows its concentration-dependent effect on surface pressure of lipid films, but in the absence of lipids its effect on pressure is independent of the position of the barrier. Heptyl AI-2 (D) behaves more like insoluble surfactant even without lipids (panel D, dotted line), showing substantial increase of surface pressure with compression. The presence of heptyl AI-2 in the subphase strongly changes the character of lipid film compression, but even this most lipophilic analog is squeezed out the film as the molecular area approaches 60–65 Å^2. The horizontal dashed line marks the monolayer-bilayer equivalence pressure.
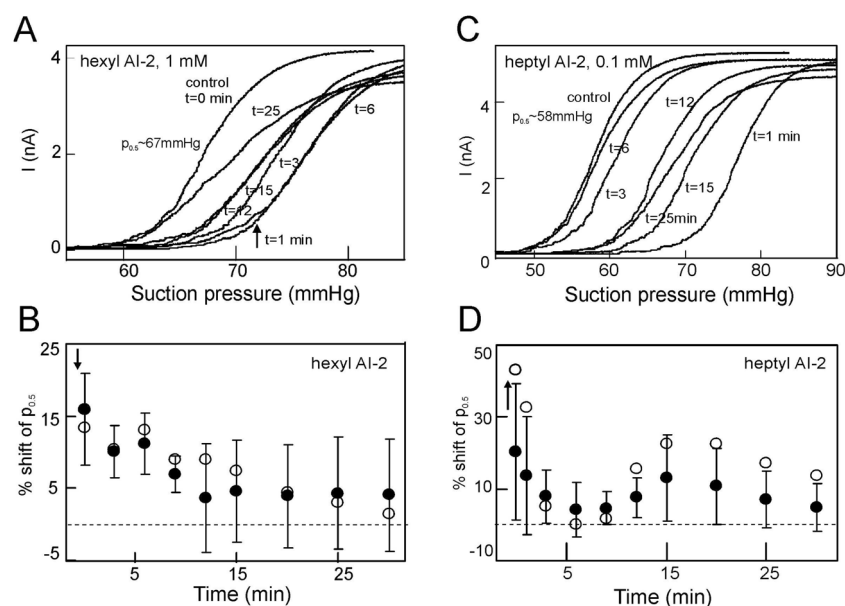
Fig. 7.
The shifts of MscS activation curves with asymmetric addition of hexyl (A, B) and hepyl (C, D) derivatives of AI-2 measured with standard 1-s saturating pressure ramps. While hexyl AI-2 in 1 mM concentration produced a transient 20% shift of $p_{0.5}$, heptyl AI-2 in 10 times lower concentration produces a 45% curve shift in that specific patch. Filled circles and error bars in (B) and (D) represent means and standard deviations for five independent experiments, whereas the open circles represent values from particular experiments presented in panels A and C. Arrows indicate the moments of AI-2 injection.

Table 1

Surface activity data for the four autoinducers obtained from molecular area calculations and from fitting the Gibbs isotherms to determine surface excess (Γ) and molecular area at the surface (A_S). Propensities toward air-water interface (K_{AW}), and the membrane partitioning coefficient (log K_{memb}) were calculated according to Suomolainen 46. Indole, AI-2 and Pentyl AI-2 showed no detectable surface activity and for this reason Γ and the following parameters are not presented.

Substance	Polar/total area, Å²	logK$_{OW}$ (computed)	Γ, mol/m²	K$_{AW}$, M^{-1}	A$_S$, Å²	log K$_{memb}$
AI-1	16/288	2.5	$3.4*10^{-6}$	$5.6*10^3$	49	1.94
Indole	75/137	2.17	NA	NA	NA	NA
AI-2 (Methyl)	74/125	−1.81	NA	NA	NA	NA
Isobutyl AI-2	74/150	−0.73	$3.5*10^{-6}$	$4.7*10^3$	48	1.91
Pentyl AI-2	74/181	0.49	NA	NA	NA	NA
Hexyl AI-2	74/195	0.64	$2.9*10^{-6}$	$2*10^4$	57	2.23
Heptyl AI-2	74/209	1.11	$2.4*10^{-6}$	$2.3*10^5$	49	3.55